Effect of Gd and Si co-doping on the band alignment and electrical properties of HfO$_2$ dielectric films prepared by atomic layer deposition

Lin Zhu[1], Xiao-Jie Liu[1], Yan-Qiang Cao[1], Ai-Dong Li[1,*] [iD], and Di Wu[1]

[1] *National Laboratory of Solid State Microstructures, Jiangsu Key Laboratory of Artificial Functional Materials, Materials Science and Engineering Department, College of Engineering and Applied Sciences, Collaborative Innovation Center of Advanced Microstructures, Nanjing University, Nanjing 210093, People's Republic of China*

ABSTRACT

Gd and Si co-doped HfO$_2$ gate dielectric thin films were prepared by atomic layer deposition (ALD), while Gd[N(SiMe$_3$)$_2$]$_3$, Hf[NEtMe]$_4$, and H$_2$O are chosen to be precursors. The Gd and Si were successfully co-doped into HfO$_2$ films using only one doping precursor Gd[N(SiMe$_3$)$_2$]$_3$. The doping concentration can be facilely tuned by controlling ALD recipe. The atomic percentages of Si/(Si + Gd + Hf) and Gd/(Si + Gd + Hf) increase from 11.5 to 28.9% and from 6.8 to 28.4% when changing the ALD cycle ratio of Gd$_x$Si$_y$O to HfO$_2$ from 1:9 to 1:1. The band gap and band alignment were investigated by X-ray photoelectron spectroscopy. The results imply that the band gap of Gd/Si co-doped HfO$_2$ films has a positive relation with doping concentration. Moreover, the valence band offset decreases with doping concentration first but then increases, while the change of conduction band offset is opposite. The (1:6)-Hf$_x$Gd$_y$Si$_z$O films with 11.6 at.% Gd/(Gd + Hf) exhibit the maximum accumulation capacitance and dielectric constant, which are only slightly smaller than those of the HfO$_2$ films. Compared to HfO$_2$ films, the leakage current density of (1:6)-Hf$_x$Gd$_y$Si$_z$O films is decreased by at least one order of magnitude. Therefore, Gd and Si co-doping can improve the electrical properties of HfO$_2$ films.

1 Introduction

Since portable electronic products come into public daily life, the dimension of Si-based metal–oxide–semiconductor field-effect-transistor (MOSFET) devices keeps continuous scaling down following *Moore's law* [1]. In the past decades, SiO$_2$-based gate dielectric was employed in the mass production of MOSFETs [2, 3]. However, the physical thickness of this insulator layer has been decreased to its physical

Lin Zhu and Xiao-Jie Liu correspond equally to this work.

Address correspondence to E-mail: adli@nju.edu.cn

Springer

limit, leading to power consumption and reliability issues due to the quantum tunneling effect [4, 5]. To solve the above issues, one of the promising ways is replacing the SiO_2 by a physically thicker layer with a higher dielectric constant dielectric films [4, 6]. Various metal oxides have been applied as high-k gate dielectrics, including ZrO_2 [7], Y_2O_3 [8], HfO_2 [9], Ta_2O_5 [10], Al_2O_3 [11], and MgO [12]. Besides inorganic materials, a kind of organic–inorganic hybrid films as high-k dielectrics can also exhibit excellent properties, such as SiO_2-TiO_2-PVP and $BaTiO_3$-PMMA-PVP, which show great application potential in flexible electronics [13, 14]. Among various high-k gate dielectric films, HfO_2 with high dielectric constant has been demonstrated to be the most capable substitute for SiO_2 to improve device performance [15–17]. Normally, gate dielectric films are expected to remain stay amorphous after a conventional activation annealing ($\sim$1000 °C), concerning that grain boundaries may serve as the paths for dopant diffusion and current leakage. Nevertheless, the crystallization temperature of pure HfO_2 is too low ($\sim$ 500 °C) [18, 19]. Si doping has been reported to suppress the crystallization of HfO_2; however, Si dopant might deteriorate the dielectric constant of HfO_2 films [20, 21]. On the other hand, it has been demonstrated that Gd doping can enhance the permittivity of HfO_2 films [22, 23]. Therefore, co-doping of Gd and Si might be an effective approach to enhance comprehensive electrical properties of HfO_2 films.

Atomic layer deposition (ALD) is one of the promising thin film deposition techniques, which is based on sequential self-limited and complementary surface chemisorption reactions. ALD possesses unique advantages such as large area uniformity, three-dimensional conformality, precise and facile thickness control down to sub-nanometer, low processing temperature, and extremely low damage to the substrate surface [24–26]. Therefore, ALD has attracted great attention in the surface engineering and nanostructure fabrication in recent years [27–29]. Amorphous gate dielectric films are preferred because grain boundaries can act as diffusion path for impurity and leakage current. Furthermore, smoother surfaces and associated improved interface quality can be achieved using amorphous gate dielectric films [5, 30]. ALD has been demonstrated widely to produce amorphous gate dielectric films with excellent interface; hence, ALD is one of the leading technologies for the high dielectric constant gate insulators deposition [31–33]. The use of Si-containing rare-earth (RE) precursors of tris[bis(trimethylsilyl)amino]RE {RE[N(SiMe$_3$)$_2$]$_3$, where RE = La [34–36], Pr [37], Lu [38], and Me = CH_3} has been reported to prepare RE silicate by ALD, which is a promising way to intentionally incorporate Si in rare-earth oxides. Therefore, Gd and Si co-doped HfO_2 ($Hf_xGd_ySi_zO$) films were deposited by ALD, and Gd[N(SiMe$_3$)$_2$]$_3$ was the only doping precursor in this work. The doping concentration tuning can be achieved by changing the ALD cycle ratio of Gd_xSi_yO to HfO_2. The effect of doping concentration of Gd and Si on the band alignment and electrical characteristics of the doped HfO_2 films were investigated systematically.

2 Experimental section

Substrates used in this work were B-doped p-type Si (100) with resistivity of 1–10 Ω cm. Prior to ALD dielectric films deposition, they were first degreased in ethanol for 5 min by sonication. Then, the Si surface native oxide was removed with 2% diluted hydrofluoric acid solution for 3 min. Finally, the substrates were blown dry with N_2 after rinsing by de-ionized water. The substrates were then transferred into the ALD chamber (Picosun SUNALE^{TM} R200 Advanced, Finland) to deposit the $Hf_xGd_ySi_zO$ films at 300 °C. The $Hf_xGd_ySi_zO$ ALD process was performed by combining HfO_2 ALD process, using Hf[NEtMe]$_4$ and H_2O, with the Gd_xSi_yO ALD process, using Gd[N(SiMe$_3$)$_2$]$_3$ and H_2O. Pure N_2 (99.999%) was used as both carrier gas and purge gas. During deposition process, the temperature of Hf[NEtMe]$_4$ and Gd[N(SiMe$_3$)$_2$]$_3$ precursors was set as 120 °C and 180 °C to ensure sufficient vapor pressure, while H_2O was kept at room temperature. Pulse time of all precursors was 0.3 s, after which was a 6 s N_2 flow step to blow reaction by-products and redundant precursors away. The composition of $Hf_xGd_ySi_zO$ films was tuned via changing the ALD recipe. Eight kinds of $Hf_xGd_ySi_zO$ samples with various compositions were prepared by depositing the alternate layers of Gd_xSi_yO and HfO_2 with Gd_xSi_yO as the beginning layer. For example, (1:N)-$Hf_xGd_ySi_zO$ films were using Gd_xSi_yO (1 cycle) + HfO_2 (N cycles, N = 1, 2, 3, 4, 5, 6, 7, 9) as one loop. The loops were varied to control the thickness of $Hf_xGd_ySi_zO$ films

as ∼ 10.7 nm. Pure Gd_xSi_yO and HfO_2 films were also prepared for comparison. The related process details are presented in Table 1. The entire sample preparation process was conducted in the clean room.

The chemical composition of $Hf_xGd_ySi_zO$ films were measured by X-ray photoelectron spectroscopy (XPS, Thermo Fisher K-Alpha) with a monochromatic Al Kα source (hv = 1486.6 eV). The excited photoelectrons were collected at a takeoff angle of 90°. The binding energy scale was calibrated using C1s peak at 284.6 eV. In addition, the valence band spectra and the O1s electron energy loss spectra of the $Hf_xGd_ySi_zO$ films were also measured by XPS to achieve the band alignment information. Pt top gate electrodes with an area of 1.54×10^{-4} cm^2 were fabricated on the surface of the $Hf_xGd_ySi_zO$ films using a shadow mask by sputtering. Capacitance–voltage (C–V) and leakage current density–voltage (J–V) characteristics tests were conducted by a Keithley 4200 semiconductor characterization system at room temperature in a closed Cascade Summit 11000B-M probe station.

3 Results and discussion

The $Hf_xGd_ySi_zO$ ALD process is illustrated in Fig. 1a, where the composition of $Hf_xGd_ySi_zO$ films can be facilely tuned by controlling the ratio of Gd_xSi_yO to HfO_2 ALD cycles. XPS was applied to determine the composition of various $Hf_xGd_ySi_zO$ films, and the typical XPS survey spectrum for (1:6)-$Hf_xGd_ySi_zO$ film is presented in Fig. 1b. The C1s, Hf 4f, Gd 4d, Si 2p, and O1s peaks located at 284.6 eV, 17.5 eV, 143.2 eV, 102.2 eV, and 530.6 eV can be easily discerned, confirming that both Gd and Si from $Gd[N(SiMe_3)_2]_3$ source can be doped into HfO_2 films. Furthermore, the chemical composition of various $Hf_xGd_ySi_zO$ films gained from XPS are summarized

in Table 1. Figure 1c plots the relationship between the doping concentration (Gd/(Gd + Si + Hf) at.% and Si/(Gd + Si + Hf) at.%) and ALD cycle ratio of $Gd_xSi_yO/(Gd_xSi_yO + HfO_2)$. It can be also seen that the Gd and Si co-doping concentrations can be elaborately tuned over a wide range by the ALD cycle ratio of Gd_xSi_yO and HfO_2. As a result, the $Hf_xGd_ySi_zO$ films with Si/(Si + Gd + Hf) at.% between 11.5 and 28.9% and Gd/(Si + Gd + Hf) at.% between 6.8 and 28.4% can be achieved via changing the ALD cycle ratio of Gd_xSi_yO/HfO_2 from 1:9 to 1:1. To avoid the effects from the silicon substrate during XPS measurement, the composition of pristine Gd_xSi_yO film on Ge substrate was also detected by XPS, as shown in the inset of Fig. 1c. Si 2p signal can still be detected, and the Si/(Si + Gd) at.% is around 40%, which is in accord with the results of pristine Gd_xSi_yO on Si substrate. Therefore, it can be demonstrated that the Si XPS signals of $Hf_xGd_ySi_zO$ samples attribute to Si dopant in $Hf_xGd_ySi_zO$ films rather than Si substrates.

The band offsets at $Hf_xGd_ySi_zO$/Si interface were also explored by XPS. The valence band offset (VBO, ΔE_v) can be determined by Kraut's method, assuming that the energy difference between the core level and the valence band (VB) edge of the substrate keeps unchanged after dielectrics films deposition [39, 40]. Thus, valence band maximum (VBM) of Si (E_{VBM}(Si)) was chosen as the reference to determine the VBO between the $Hf_xGd_ySi_zO$ films and the Si substrate. Figure 2a shows the XPS valence band spectra of the Si substrate and the $Hf_xGd_ySi_zO$ films deposited on Si substrates. The VBM of the clean Si substrate (E_{VBM}(Si)) has been determined to be 0.52 eV by using the linear extrapolation as shown in Fig. 2a [41, 42]. The VBMs of the (1:N)-$Hf_xGd_ySi_zO$/Si samples (E_{VBM}($Hf_xGd_ySi_zO$)) are determined to be 3.12 eV, 3.09 eV, 2.72 eV, 2.71 eV, 2.77 eV, 2.77 eV, 3.08 eV, and 3.19 eV, respectively. Therefore, the

**Table 1** Process details and composition of (1:N)-$Hf_xGd_ySi_zO$, Gd_xSi_yO, and HfO_2 samples

Gd/Hf cycle ratio	1:0	1:1	1:2	1:3	1:4	1:5	1:6	1:7	1:9	0:1
Loops	153	63	40	29	23	19	16	14	11	107
Total cycles	153	126	120	116	115	114	112	112	110	107
Si at.%	38.4	28.9	21.3	19.6	17.9	16.3	14.9	13.7	11.5	0
Gd at.%	61.6	28.4	21.3	16.0	13.4	11.8	9.9	8.8	6.8	0
Gd/(Gd + Hf) at.%	100	39.9	27.1	19.9	16.3	14.1	11.6	10.2	7.7	0

Si at.% and Gd at.% refer to the atomic percent of Si/(Si + Gd + Hf) and Gd/(Si + Gd + Hf), respectively

Fig. 1 a Schematic illustration of $Hf_xGd_ySi_zO$ ALD process, **b** XPS survey spectrum of (1:6)-$Hf_xGd_ySi_zO$ film, **c** Si/(Hf + Gd + Si), and Gd/(Hf + Gd + Si) atomic percentage versus the ALD cycle ratio of Gd_xSi_yO/(Gd_xSi_yO + HfO_2). The inset in **b** and **c** are the Si 2p XPS spectra for (1:6)-$Hf_xGd_ySi_zO$ film on Si and pristine Gd_xSi_yO films grown on Ge substrate, respectively
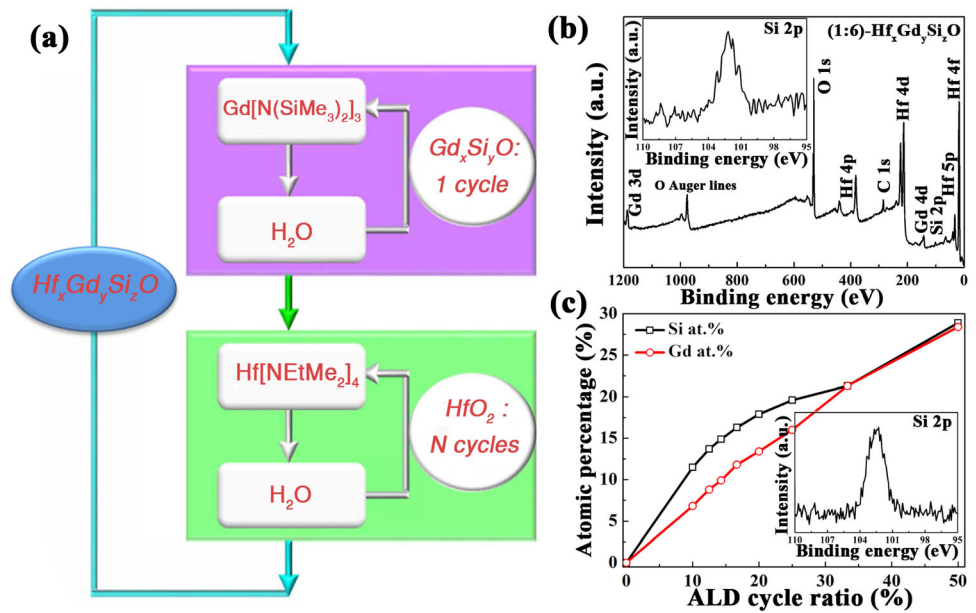
Fig. 2 a Valence band spectra and **b** O1s electron energy loss spectra of the (1:N)-$Hf_xGd_ySi_zO$/Si samples
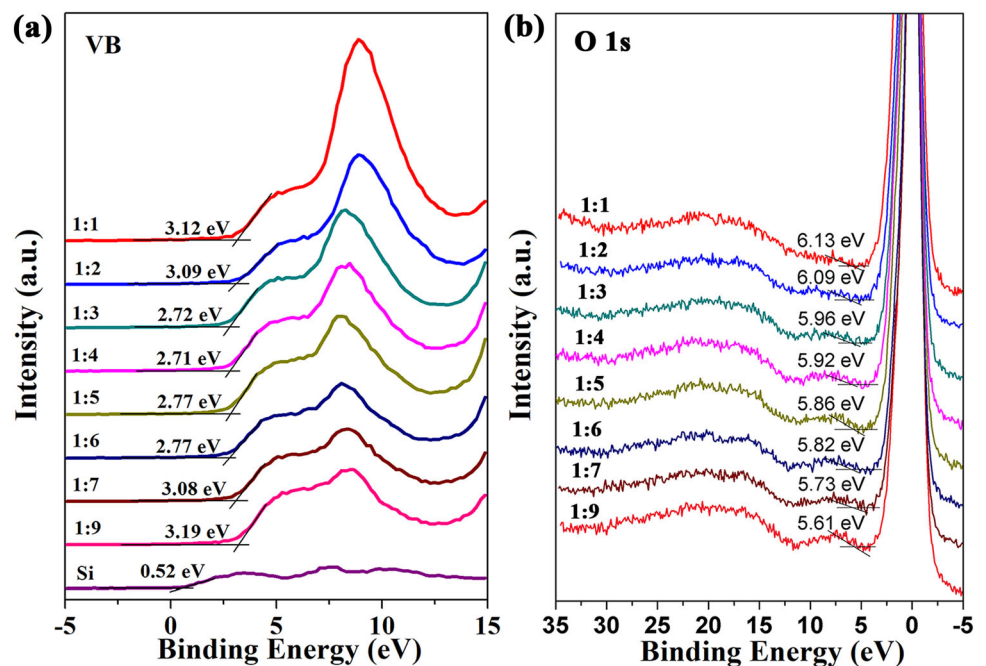
VBOs of (1:N)-$Hf_xGd_ySi_zO$/Si samples (ΔE_v($Hf_xGd_ySi_zO$/Si)) are calculated as 2.60 eV, 2.57 eV, 2.20 eV, 2.19 eV, 2.25 eV, 2.25 eV, 2.56 eV, and 2.67 eV using the following formula: ΔE_v($Hf_xGd_ySi_zO$/Si) = E_{VBM}($Hf_xGd_ySi_zO$)-E_{VBM}(Si).

The conduction band offset (CBO, ΔE_c) can be achieved by ΔE_c($Hf_xGd_ySi_zO$/Si) = E_g($Hf_xGd_ySi_zO$)-E_g(Si)-ΔE_v($Hf_xGd_ySi_zO$/Si), subtracting the band gap of the Si substrate and the VBO from the band gap of $Hf_xGd_ySi_zO$. The band gaps of $Hf_xGd_ySi_zO$ films can

be determined by the O1s electron energy loss spectra by using the linear extrapolation method [43, 44], as shown in Fig. 2b. Thus, the band gaps of the (1:N)-$Hf_xGd_ySi_zO$ films (E_g($Hf_xGd_ySi_zO$)) can be determined to be 6.13 eV, 6.09 eV, 5.96 eV, 5.92 eV, 5.86 eV, 5.82 eV, 5.73 eV, and 5.61 eV, respectively. Therefore, the CBOs of (1:N)-$Hf_xGd_ySi_zO$/Si samples (ΔE_c($Hf_xGd_ySi_zO$/Si)) are estimated to be 2.41 eV, 2.40 eV, 2.64 eV, 2.61 eV, 2.49 eV, 2.45 eV, 2.05 eV, and 1.82 eV, respectively.

According to the band gaps, VBOs, and CBOs results, the schematic band alignment diagram of the $(1:N)$-$Hf_xGd_ySi_zO/Si$ heterostructures is constructed, as shown in Fig. 3. The band structures indicate that the band gap increases with doping concentration, which may attribute to the existence of Gd–O–Hf bonding and Si–O bonding [23]. In addition, the VBO decreases first and then increases, and the CBO increases first and then decreases along with the Gd/Hf atomic ratio rising. Therefore, the band offsets symmetry of $Hf_xGd_ySi_zO/Si$ heterostructures can be improved by tuning the composition of $Hf_xGd_ySi_zO$. For example, $(1:6)$-$Hf_xGd_ySi_zO$ films exhibit both large VBO (2.25 eV) and CBO (2.45 eV) values, beneficial for inhibiting the leakage current by huge barrier heights.

The MOS capacitors with the same physical thickness of $(1:N)$-$Hf_xGd_ySi_zO$ films on Si substrates were fabricated. The high-frequency (1 MHz) C–V characteristics of these capacitors were measured. The accumulation capacitances of these $Pt/(1:N)$-$Hf_xGd_ySi_zO/Si$ capacitors are 0.93, 1.01, 1.08, 1.04, 0.98, 0.83, 0.82, and 0.76 μF cm^{-2}, respectively. Considering the $Gd/(Gd + Hf)$ atomic percent of the $(1:N)$-$Hf_xGd_ySi_zO$ films in Table 1, the accumulation capacitance as a function of the $Gd/(Gd + Hf)$ atomic percentage is plotted in Fig. 4. The results indicate that the accumulation capacitance increases first and then decreases along with doping concentration. Thus, the $Hf_xGd_ySi_zO$ films with $Gd/(Gd +$ Hf) of 11.6 at.% exhibit the maximum accumulation capacitance and dielectric constant. Our results are consistent with previous literature by Adelmann et al. [45], which reported that Gd-doped HfO_2 films with the doping concentration of 11.1 at.% exhibit the maximum dielectric constant.

Figure 5a, b compares the high-frequency (1 MHz) C–V and J–V characteristics of $(1:6)$-$Hf_xGd_ySi_zO$ films and HfO_2 films, respectively. The accumulation capacitance densities of $(1:6)$-$Hf_xGd_ySi_zO$ films and HfO_2 films are 1.08 μF cm^{-2} and 1.17 μF cm^{-2}, which can be extracted from Fig. 5a. The calculated relative dielectric constant of the $(1:6)$-$Hf_xGd_ySi_zO$ films is 13.3, which is only slightly smaller than that of the HfO_2 films (14.4). According to Fig. 5b, it can be observed that the leakage current density of $(1:6)$-$Hf_xGd_ySi_zO$ films and HfO_2 films at gate voltage of − 1 V are 1.22×10^{-4} A cm^{-2} and 2.62×10^{-3} A cm^{-2}, respectively. Compared to HfO_2 films, the leakage current density of $(1:6)$-$Hf_xGd_ySi_zO$ films is lower with more than an order of magnitude. Therefore, comprehensive electrical properties of HfO_2 films can be improved by Gd and Si co-doping, reducing the leakage current density effectively without deteriorating the dielectric constant obviously. Furthermore, the current density of $Hf_xGd_ySi_zO/Si$ heterostructures as a function of $Gd/(Gd + Hf)$ atomic percentage was also provided, as shown in the inset of Fig. 5b. It can be seen that (1:3), (1:5), and $(1:6)$-$Hf_xGd_ySi_zO$ films all can exhibit a decreased current density due to their both large VBO and CBO. However, the $(1:9)$-$Hf_xGd_ySi_zO$ film
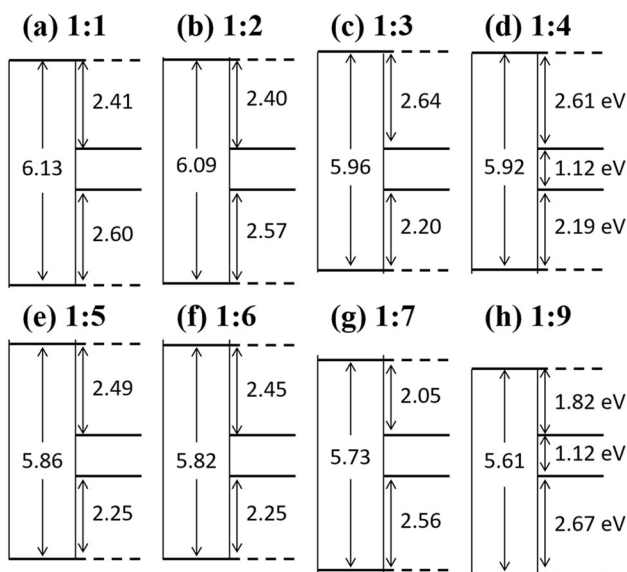
Fig. 3 The schematic band structure diagram of the $(1:N)$-$Hf_xGd_ySi_zO/Si$ heterostructures
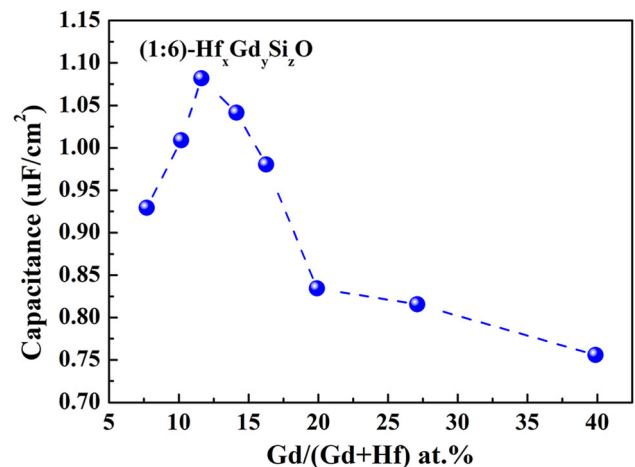
Fig. 4 Accumulation capacitance of the $Hf_xGd_ySi_zO$ films on Si substrates as a function of the $Gd/(Gd + Hf)$ atomic percentage
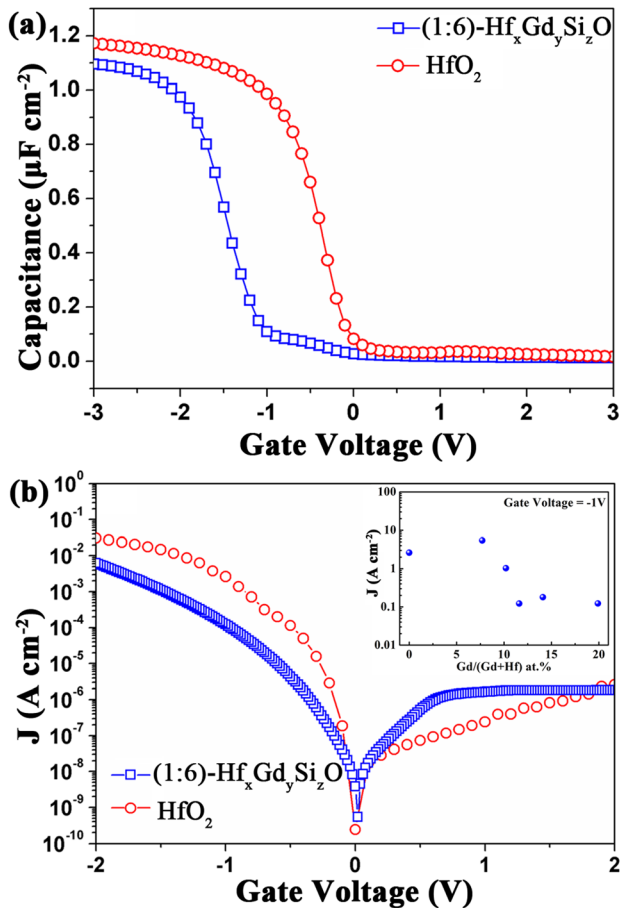
Fig. 5 **a** C–V and **b** J–V characteristics of (1:6)-Hf$_x$Gd$_y$Si$_z$O films and HfO$_2$ films on Si substrates. The inset of **b** is the leakage current density of the Hf$_x$Gd$_y$Si$_z$O films on Si substrates as a function of the Gd/(Gd + Hf) atomic percentage

still shows a large current density, which may be ascribed to its small CBO.

4 Conclusion

Gd and Si co-doped HfO$_2$ films (Hf$_x$Gd$_y$Si$_z$O) were successfully deposited by ALD in this work. XPS results demonstrate that Gd and Si can be co-doped into HfO$_2$ films using the only doping precursor Gd[N(SiMe$_3$)$_2$]$_3$. By tuning the ALD cycle ratio, the atomic percentages of Si/(Si + Gd + Hf), Gd/(Si + Gd + Hf) and Gd/(Gd + Hf) can be tuned between 11.5 and 28.9, 6.8 and 28.4, and 7.7 and 39.9%, respectively. The band alignment and electrical properties of ALD Hf$_x$Gd$_y$Si$_z$O films on Si substrates with different doping concentrations were investigated. With increasing the Gd/Si doping

concentration, the band gap increases, the VBO value decreases first and then increases, while the CBO value increases first and then decreases. Thus, (1:6)-Hf$_x$Gd$_y$Si$_z$O films achieve the best band offset symmetry with both large VBO (2.25 eV) and CBO (2.45 eV). The (1:6)-Hf$_x$Gd$_y$Si$_z$O films with 11.6 at.% Gd/(Gd + Hf) exhibit the maximum accumulation capacitance and dielectric constant which are only slightly smaller than those of the HfO$_2$ films. Compared to HfO$_2$ films, the leakage current density of (1:6)-Hf$_x$Gd$_y$Si$_z$O films is decreased by at least one order of magnitude. Above results indicate that co-doping of Si and Gd maybe a promising way to improve comprehensive electrical properties of HfO$_2$ films, effectively reducing the leakage current density while maintaining high dielectric constant.

Compliance with ethical standards

Conflict of interest   The authors declare that there is no conflict of interest.

References

1. G.E. Moore, Cramming more components onto integrated circuits, Reprinted from Electronics **38**(8), April 19, 1965, pp.114 ff; IEEE Solid State Circuits Newsl. **11**, 33–35 (2006)
2. J.-S. Kim, A.M. Tyryshkin, S.A. Lyon, Annealing shallow Si/SiO$_2$ interface traps in electron-beam irradiated high-mobility metal-oxide-silicon transistors. Appl. Phys. Lett. **110**, 123505 (2017)
3. M.L. Green, E.P. Gusev, R. Degraeve, E.L. Garfunkel, Ultrathin (<4 nm) SiO$_2$ and Si-O-N gate dielectric layers for silicon microelectronics: Understanding the processing, structure, and physical and electrical limits. J. Appl. Phys. **90**, 2057–2121 (2001)
4. J. Robertson, R.M. Wallace, High-K materials and metal gates for CMOS applications. Mater. Sci. Eng. R **88**, 1–41 (2015)
5. G.D. Wilk, R.M. Wallace, J.M. Anthony, High-κ gate dielectrics: Current status and materials properties considerations. J. Appl. Phys. **89**, 5243–5275 (2001)

6. D.G. Schlom, S. Guha, S. Datta, Gate Oxides Beyond SiO_2. MRS Bull. **33**, 1017–1025 (2011)

7. A. Liu, High-performance fully amorphous bilayer metal-oxide thin film transistors using ultrathin solution-processed ZrO_x dielectric. Appl. Phys. Lett. **105**, 113509 (2014)

8. G. Liu, A. Liu, H. Zhu, B. Shin, E. Fortunato, R. Martins, Y. Wang, F. Shan, Low-temperature, nontoxic water-induced metal-oxide thin films and their application in thin-film transistors. Adv. Funct. Mater. **25**, 2564–2572 (2015)

9. X.-F. Li, X.-J. Liu, Y.-Q. Cao, A.-D. Li, H. Li, D. Wu, Improved interfacial and electrical properties of atomic layer deposition HfO_2 films on Ge with La_2O_3 passivation. Appl. Surf. Sci. **264**, 783–786 (2013)

10. L. Pereira, P. Barquinha, E. Fortunato, R. Martins, D. Kang, C.J. Kim, H. Lim, I. Song, Y. Park, High k dielectrics for low temperature electronics. Thin Solid Films **516**, 1544–1548 (2008)

11. P. Ma, L. Du, Y. Wang, R. Jiang, Q. Xin, Y. Li, A. Song, Low voltage operation of IGZO thin film transistors enabled by ultrathin Al_2O_3 gate dielectric. Appl. Phys. Lett. **112**, 023501 (2018)

12. G. Jiang, A. Liu, G. Liu, C. Zhu, Y. Meng, B. Shin, E. Fortunato, R. Martins, F. Shan, Solution-processed high-k magnesium oxide dielectrics for low-voltage oxide thin-film transistors. Appl. Phys. Lett. **109**, 183508 (2016)

13. H. Najafi-Ashtiani, Performance evaluation of free-silicon organic-inorganic hybrid (SiO_2-TiO_2-PVP) thin films as a gate dielectric. Appl. Surf. Sci. **455**, 373–378 (2018)

14. H. Najafi-Ashtiani, Low temperature processing of $BaTiO_3$-PMMA-PVP hybrid films as transparent dielectric gate. J. Mater. Sci.-Mater. El. **30**, 7087–7094 (2019)

15. C. Liu, Z. Wang, H. Lu, Y. Zhang, D. Liu, Y.-M. Zhang, Z. Ma, J. Zhao, L. Guo, K. Xiong, Atomic-layer-deposited HfO_2/Al_2O_3 laminated dielectrics for bendable Si nanomembrane based MOS capacitors. Appl. Phys. Lett. **114**, 142903 (2019)

16. A. Kumar, S. Mondal, K.S.R.K. Rao, Tunable band alignment and dielectric constant of solution route fabricated Al/HfO_2/Si gate stack for CMOS applications. J. Appl. Phys. **121**, 085301 (2017)

17. G. Venkata Rao, M. Kumar, T.V. Rajesh, D.V. Rama Koti Reddy, D. Anjaneyulu, B. Sainath, S.V. Jagadeesh Chandra, Investigations on the nitride interface engineering at HfO_2/Ge stacks for MOS devices. Mater. Today **5**, 650–657 (2018)

18. G. Tian, S. Wu, K. Shu, L. Qin, J. Shao, Influence of deposition conditions on the microstructure of oxides thin films. Appl. Surf. Sci. **253**, 8782–8787 (2007)

19. Y. Yamamoto, K. Kita, K. Kyuno, A. Toriumi, Structural and electrical properties of $HfLaO_x$ films for an amorphous high-k gate insulator. Appl. Phys. Lett. **89**, 032903 (2006)

20. R.E. Sah, Silicon nitride, silicon dioxide thin insulating films, and other emerging dielectrics, in *VIII: Proceedings of the International Symposium* (The Electrochemical Society, City, 2005)

21. G.D. Wilk, R.M. Wallace, J.M. Anthony, Hafnium and zirconium silicates for advanced gate dielectrics. J. Appl. Phys. **87**, 484–492 (2000)

22. Y. Xiong, H. Tu, J. Du, M. Ji, X. Zhang, L. Wang, Band structure and electrical properties of Gd-doped HfO_2 high k gate dielectric. Appl. Phys. Lett. **97**, 5243 (2010)

23. X.J. Liu, A.D. Li, X. Qian, J.Z. Kong, J. Zhou, D. Wu, First-principles study on electronic structure of Gd-doped HfO_2 high k gate dielectrics. Integr. Ferroelect. **134**, 3–9 (2012)

24. S.M. George, Atomic layer deposition: an overview. Chem. Rev. **110**, 111–131 (2010)

25. V. Miikkulainen, M. Leskelä, M. Ritala, R.L. Puurunen, Crystallinity of inorganic films grown by atomic layer deposition: overview and general trends. J. Appl. Phys. **113**, 021301 (2013)

26. R.L. Puurunen, Surface chemistry of atomic layer deposition: a case study for the trimethylaluminum/water process. J. Appl. Phys. **97**, 121301 (2005)

27. X. Meng, X.-Q. Yang, X. Sun, Emerging applications of atomic layer deposition for lithium-ion battery Studies. Adv. Mater. **24**, 3589–3615 (2012)

28. X. Meng, X. Wang, D. Geng, C. Ozgitakgun, N. Schneider, J.W. Elam, Atomic layer deposition for nanomaterials synthesis and functionalization in energy technology. Mater. Horiz. **4**, 133–154 (2017)

29. M. Knez, K. Nielsch, L. Niinistö, Synthesis and surface engineering of complex nanostructures by atomic layer deposition. Adv. Mater. **19**, 3425–3438 (2007)

30. P. Barquinha, L. Pereira, G. Goncalves, R. Martins, E. Fortunato, Performance and stability of low temperature transparent thin-film transistors using amorphous multicomponent dielectrics. J. Electrochem. Soc. **156**, H824 (2009)

31. G. Lin, M.-Q. Zhao, M. Jia, J. Zhang, P. Cui, L. Wei, H. Zhao, A.T.C. Johnson, L. Gundlach, Y. Zeng, Performance enhancement of monolayer MoS_2 transistors by atomic layer deposition of high-k dielectric assisted by Al_2O_3 seed layer. J. Phys. D **53**, 105103 (2019)

32. Y.H. Park, M.H. Kim, S.B. Kim, H.J. Jung, K. Chae, Y.H. Ahn, J.-Y. Park, F. Rotermund, S.W. Lee, Enhanced nucleation of high-k dielectrics on graphene by atomic layer deposition. Chem. Mater. **28**, 7268–7275 (2016)

33. Y.-Q. Cao, J. Chen, X.-J. Liu, X. Li, Z.-Y. Cao, Y.-J. Ma, D. Wu, A.-D. Li, HfO_2/GeO_xN_y/Ge gate stacks with sub-nanometer capacitance equivalent thickness and low interface trap density by in situ NH_3 plasma pretreatment. Appl. Surf. Sci. **325**, 13–19 (2015)

34. D.H. Triyoso, R.I. Hegde, J. Grant, P. Fejes, P.J. Tobin, Film properties of ALD HfO_2 and La_2O_3 gate dielectrics grown on Si with various pre-deposition treatments. J. Vac. Sci. Technol. B. **22**, 2121–2127 (2004)

35. D.H. Triyoso, R.I. Hegde, J.M. Grant, J.K. Schaeffer, D. Roan, B.E. White Jr., P.J. Tobin, Evaluation of lanthanum based gate dielectrics deposited by atomic layer deposition. J. Vac. Sci. Technol. B. **23**, 288–297 (2005)

36. Y.J. Choi, S.-J. Won, H.-S. Jung, Effects of oxygen source on film properties of atomic-layer-deposited La-silicate film using $La[N(SiMe_3)_2]_3$. ECS Solid State Lett. **1**, N4 (2012)

37. K. Kukli, M. Ritala, T. Pilvi, T. Sajavaara, M. Leskela, A.C. Jones, H.C. Aspinall, D.C. Gilmer, P.J. Tobin, Evaluation of a praseodymium precursor for atomic layer deposition of oxide dielectric films. Chem. Mater. **16**, 5162–5168 (2004)

38. G. Scarel, C. Wiemer, G. Tallarida, S. Spiga, G. Seguini, E. Bonera, M. Fanciulli, Y. Lebedinskii, A. Zenkevich, G. Pavia, Atomic layer deposition of Lu silicate films using $[(Me_3Si)_2N]_3Lu$. J. Electrochem. Soc. **153**, F271 (2006)

39. E. Kraut, R. Grant, J. Waldrop, S. Kowalczyk, Precise determination of the valence-band edge in x-ray photoemission spectra: application to measurement of semiconductor interface potentials. Phys. Rev. Lett. **44**, 1620 (1980)

40. Y. Mi, S. Wang, J. Chai, J. Pan, A. Huan, M. Ning, C. Ong, Energy-band alignments at $LaAlO_3$ and Ge interfaces. Appl. Phys. Lett. **89**, 2107 (2006)

41. S.A. Chambers, Y. Liang, Z. Yu, R. Droopad, J. Ramdani, K. Eisenbeiser, Band discontinuities at epitaxial SrTiO3/Si(001) heterojunctions. Appl. Phys. Lett. **77**, 1662 (2000)

42. R. Mahapatra, A.K. Chakraborty, A.B. Horsfall, N.G. Wright, G. Beamson, K.S. Coleman, Energy-band alignment of HfO_2/SiO_2/SiC gate dielectric stack. Appl. Phys. Lett. **92**, 1830 (2008)

43. S. Miyazaki, Photoemission study of energy-band alignments and gap-state density distributions for high-k gate dielectrics. J. Vac. Sci. Technol. B. **19**, 2212–2216 (2001)

44. H.Y. Yu, M.F. Li, D.L. Kwong, ALD $(HfO_2)_x(Al_2O_3)_{1-x}$ high-k gate dielectrics for advanced MOS devices application. Thin Solid Films **462**, 110–113 (2004)

45. C. Adelmann, H. Tielens, D. Dewulf, A. Hardy, D. Pierreux, J. Swerts, E. Rosseel, X. Shi, M. Van Bael, J.A. Kittl, Atomic layer deposition of Gd-doped HfO_2 thin films. J. Electrochem. Soc. **157**, G105 (2010)